The International Journal of Advanced Manufacturing Technology (2019) 104:617–629
https://doi.org/10.1007/s00170-019-03924-7

ORIGINAL ARTICLE

An optimized single-point offset method for reducing the theoretical error of S-shaped test piece

Haohao Tao[1] · Jinwei Fan[1] · Changjun Wu[1] · Ri Pan[1]

Received: 14 October 2018 / Accepted: 21 May 2019 / Published online: 6 June 2019

Abstract
The S-shaped test piece is utilized to comprehensively detect the machining accuracy of multi-axis machine tools. However, due to the existence of the influence of theoretical error for S-shaped test piece on the acceptance of multi-axis machine tools, therefore, a new methodology to reduce the theoretical error is proposed in this study. Firstly, the uniform double cubic B-spline surface model is applied to a surface representation. By utilizing this model, a model of the S-shaped test piece is established. Furthermore, the distribution of the twist angle at the selected three section lines is obtained. Meanwhile, the influence of twist angle on the theoretical error of S-shaped test pieces is analyzed. Then, the single-point offset (SPO) method is analyzed, which has some drawbacks. In order to significantly reduce the theoretical error of S-shaped test piece, the optimized single-point offset (OSPO) method is proposed. Moreover, the tool path of the S-shaped test piece is generated by CAD/CAM software based on the OSPO method. Finally, in order to verify the feasibility of the presented method, a machining and measurement experiment is carried out on the gantry-type five-axis milling machine tool (XKAS2525) and coordinate measuring machine (CMM) based on the S-shaped test piece, respectively. Experiment results show that the average theoretical error of S-shaped test pieces based on the OSPO method is reduced by about 50.1% than that on the SPO method. In addition, the vast majority of theoretical errors based on the OSPO method are approximately less than 5 μm, which can be negligible. It is therefore reasonable to conclude that, compared with the SPO method, the proposed method in this paper can avoid the influence of theoretical error on the acceptance of multi-axis machine tools intuitively and efficiently.

Keywords Multi-axis machine tools · S-shaped test piece · Theoretical error · Twist angle · The optimized single-point offset method

1 Introduction

Multi-axis machine tools with clear advantages of higher material removal rate, lower cutting time, fewer set-ups [1, 2], better versatility, and higher machining efficiency [3] are extensively adaptable for the machining of sculptured surfaces in aerospace, military, ships, cars, and other industries [4–6]. Nevertheless, multi-axis machine tools cannot offer the same machining accuracy as their three-axis machine tools due to the additional rotary axes. Since the machining accuracy of machine tools directly reflects the accuracy of the machined workpiece, unknown precision of machine tools will lead to uncertain machining accuracy and surface quality of machined workpiece [7–11]. Therefore, how to efficiently evaluate the performance of multi-axis machine tools is of critical importance in the manufacturing community.

Considerable research work has been devoted to detect the machining accuracy of multi-axis machine tools during the past decades worldwide [12–15]. The standard ISO 10791-7 [16], whose standard test piece consists of a circle, a square, a diamond shape contour, and a 3° sided quadrilateral, aims to supply information as wide and comprehensive as possible on tests and checks and describes a machining test to assess the machining performance of machine tools. Although the performance of three-axis machine tools can be exhibited by measuring verticality, parallelism, and circularity of the standard test piece, it is not suitable for evaluating the machining performance of multi-axis machine tools. The cone frustum

✉ Jinwei Fan
jwfan@bjut.edu.cn

[1] Beijing Key Laboratory of Advanced Manufacturing Technology, Beijing University of Technology, Beijing 100124, People's Republic of China

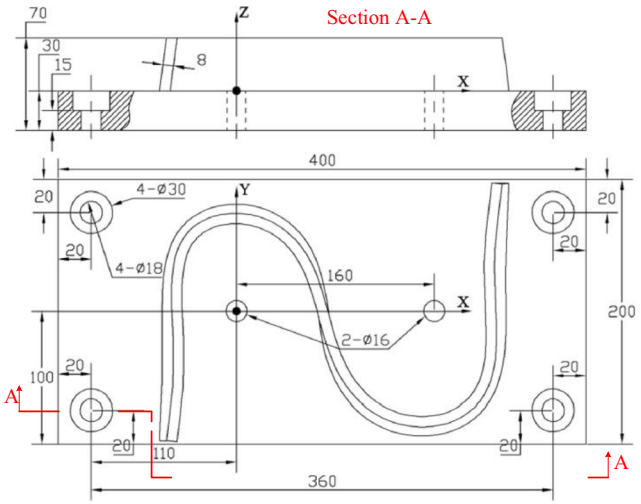

Fig. 1 Engineering drawings of S-shaped test piece

machining test, which was created by The National Aerospace Standard (NAS) 979 in 1969 [17], is the best known and extensively accepted in the machine tool industry as a final performance test for five-axis machine tools. Moreover, according to reference [18], the Numerical Control Gesellschaft (NCG) test piece has been developed to characterize complex curved surfaces feature. The above test pieces are utilized to exhibit the performance of machine tools. However, since the characteristics of complex curved surfaces, such as the conversion of open and close angle, variable curvature, and thin-wall, are different from the characteristics of NAS979 frustum test piece, poor machining accuracy and unsmooth contour are frequently obtained while processing parts with sculptured surfaces, despite multi-axis machine tools having been qualified by NAS979 frustum test piece. In addition, although the NCG test piece integrates numerous characteristics associated with sculptured surfaces, it cannot be popularly applied to evaluate the machining performance of multi-axis machine tools due to its complex model and time-consuming processing.

In order to address the above problems and comprehensively exhibit the machining accuracy of multi-axis machine tools, it is of great theoretical and practical significant to develop a new test piece. Hence, a novel "S" shaped detection test piece, called S-shaped test piece, was developed by Chengdu Aircraft Industry Group [19]. S-shaped test piece has already

Table 1 The dimension and material parameters of the S-shaped test piece

The external dimensions (mm)	400 × 200
The profile dimensions (mm)	250 × 180
The height of rectangular base (mm)	30
The height of S-shaped edge strip (mm)	40
The material of S-shaped test piece	The aluminum alloy 7075

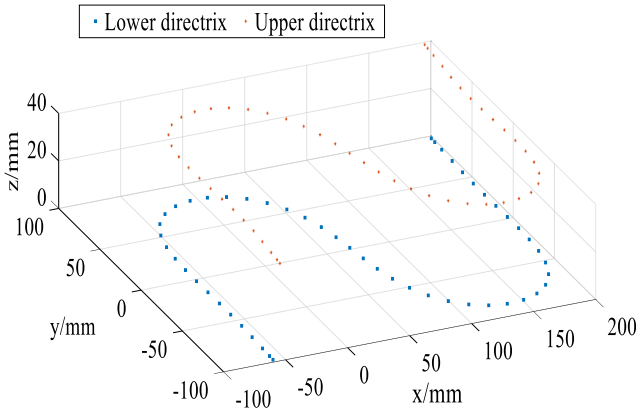

Fig. 2 Control points on the directrix

been accepted by ISO/TC39/SC2 at the 79th ISO meeting as an additional machining test in ISO 10791-7 for testing the machining accuracy of multi-axis machine tools [20]. According to reference [19], since S-shaped test piece integrates various features of sculpture surface, such as twist angle, the processing area of open angle and closed angle conversion, and variable curvature, it is a faithful representation of sculpture surface, such as aerospace structural components, turbine blades, and the key component for the diesel engine of large ships. These features have distinct advantages in detecting the machining accuracy of multi-axis machine tools than other test pieces. Therefore, research on the ability of the S-shaped test piece for evaluating the machining performance of multi-axis machine tools is of crucial importance.

According to references [21, 22], a model of the mechanical system and servo system has been set up to find out the key dynamic machine factors and develop an algorithm to track the cause of the processed error based on S-shaped test piece. Chen et al. [23] established a model of error parameter sensitivity influencing the accuracy of the curved surface and impact analysis based on the actual machining of the S-shaped sample of complex CNC machine tools, and then the five key parameters that have a great influence on machining errors are determined.

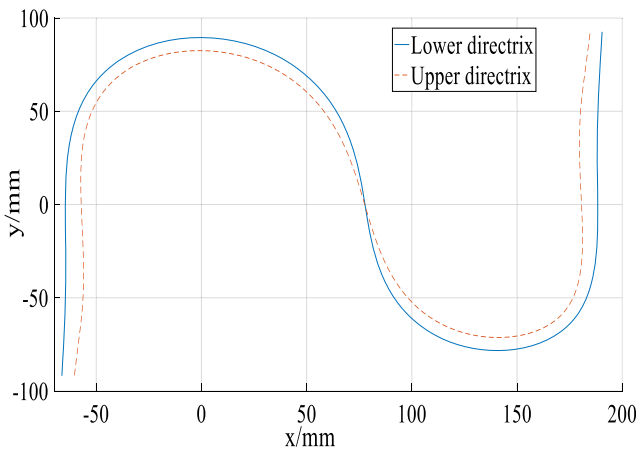

Fig. 3 The S-shaped directrix

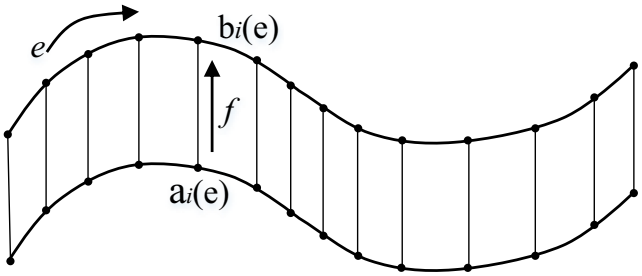

Fig. 4 Modeling method of the S-shaped ruled surface

Su and Wang [24] presented a new standard using an S-shaped test piece for evaluating the machining performance of five-axis machine tools. In order to assess the kinematic errors of five-axis machine tools, Ibaraki et al. [25] formulated a relationship between geometric errors of S-shaped test piece and the machine's kinematic errors and carried out a machining test. Jiang et al. [26] found out the cause of surface morphology abnormality at machined "S" test piece by analyzing the geometric and machining features of "S" test piece.

As can be observed in the above-mentioned studies, considerable research work has been devoted to analyze the influence of machine errors for machine tools on the machining accuracy of the S-shaped test piece. The theoretical errors existed in the design stage of the S-shaped test piece and are the natural property of S-shaped test piece. Due to the existence of twist angle, the direction vector of non-developed rule surface along the generatrix varies unevenly during the process of modeling of S-shaped test piece. And it can only ensure that the normal vector of non-developed rule surface coincides with the normal vector of tool surface at one point in the actual flank milling process of S-shaped test piece. Thus, it is obvious that the theoretical error exists while planning tool path. In addition, the S-shaped test piece formed by a thickening of the non-developed rule surface cannot be developed by the envelope of a cylinder with a radius greater than zero. Therefore, the theoretical error cannot be averted so long as the radius of the tool is not equal to zero.

Due to the presence of theoretical error, this interference that theoretical errors have some influence on the results of the analysis introduces mistakes, when manufacturers of machine tools use the S-shaped test piece to assess the machining

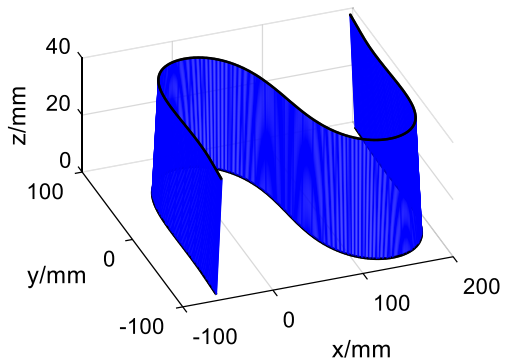

Fig. 5 Generatrix of ruled surface

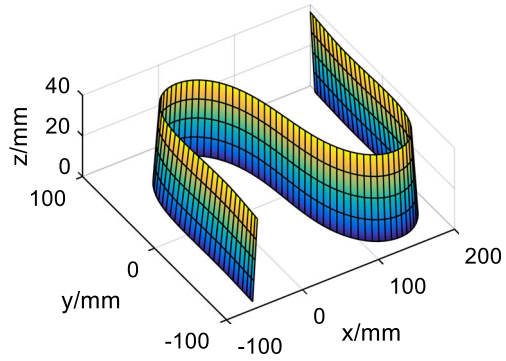

Fig. 6 Mesh of ruled surface

performance of machine tools. The performance of multi-axis machine tools cannot be comprehensively and accurately evaluated. Therefore, it is of great theoretical and practical significance to reduce the theoretical error. According to references [27, 28], the single-point offset (SPO) position method was proposed for the flank milling of the developable ruled surfaces to reduce machining error. Subsequently, in contrast to the SPO algorithm, Redonnet et al. [29, 30] introduced the three-point tangential (TPT) method to reduce machining error, and tool positions were obtained by using the CAD/CAM software. However, the machining error cannot be significantly reduced. For this reason, Bedi et al. [31] proposed the double-point tangential (DPT) method for the surface milled by using a cylindrical cutter when flank milling. According to references [32–34], the proposed NC path–generating algorithms are utilized for the reduction of geometrical deviations between the designed surface and the actual machine surface. Although these methods can produce a better solution in minimizing the deviations, the theoretical errors still exist. Guan et al. [35] used the single-point offset (SPO) position method to calculate the theoretical error of the S-shaped test piece and proposed pre-compensation (PRC) and post-compensation (POC) methods to decrease the influences of a theoretical error on the acceptance of multi-axis machine tools. Guan et al. [36] proposed the new three-point tangential (NTPT) algorithm for flank milling of S-shaped test piece.

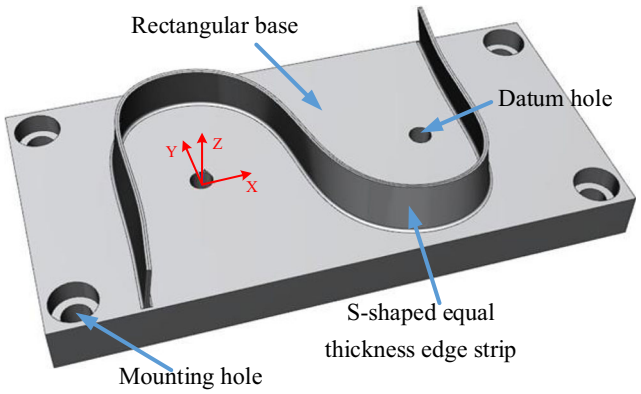

Fig. 7 The S-shaped test piece

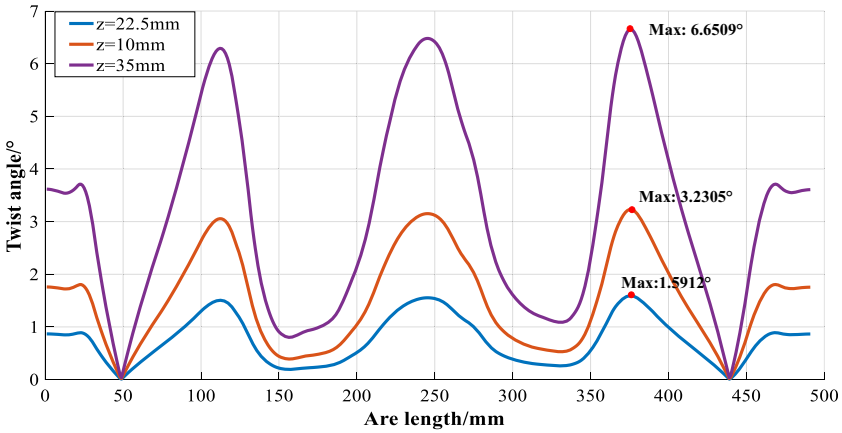

Fig. 8 The twist angle of S-shaped ruled surface obtained using the SPO method

Experiments indicate that the proposed method has extensive adaptability for different surfaces. Nevertheless, those methods are so complex that they cannot be properly applied in the CAD/CAM software for reducing the theoretical error. Therefore, it is important to propose a feasible and effective method to reduce the theoretical error.

In view of the limitations stated, first, the uniform double cubic B-spline surface model is applied to the surface representation, and a three-dimensional model of the S-shaped test piece is established based on this model. Then, in order to analyze the influence of twist angle on the theoretical error of S-shaped test piece, the distribution of twist angle is obtained. Finally, an optimized tool path offset method, the optimized single-point offset (OSPO) method, was proposed based on the conventional single-point offset method. The optimized tool path can be subsequently generated by using CAD/CAM software on the basis of the OSPO method. With the proposed method, the theoretical error of S-shaped test piece can thus be significantly reduced. Therefore, the performance of multi-axis machine tools can be comprehensively, accurately, and effectively exhibited by S-shaped test piece.

The rest of this paper is arranged as follows. A three-dimensional model of the S-shaped test piece is established based on a uniform double cubic B-spline surface in Section 2. The influence of twist angle on the theoretical error is analyzed in Section 3. The optimized single-point offset (OSPO) method is presented and compared with traditional single-point offset method in Section 4. In Section 5, an experimental study is carried out to demonstrate the effectiveness of the proposed method, and finally some conclusions are drawn in Section 6.

2 Modeling of S-shaped test piece

As illustrated in Fig. 1, the S-shaped test piece consists of an S-shaped equal thickness edge strip and a rectangular base. Thereinto, four mounting holes with a diameter of 30 mm and two datum holes with a diameter of 16 mm are utilized to install and locate for the machining and accuracy test of S-shaped test piece respectively. The dimension and material parameters of the S-shaped test piece can be seen in Table 1. According to the requirement of United States Patent, the allowable value of machining error of the S-shaped test piece is restricted within ± 0.05 mm [19].

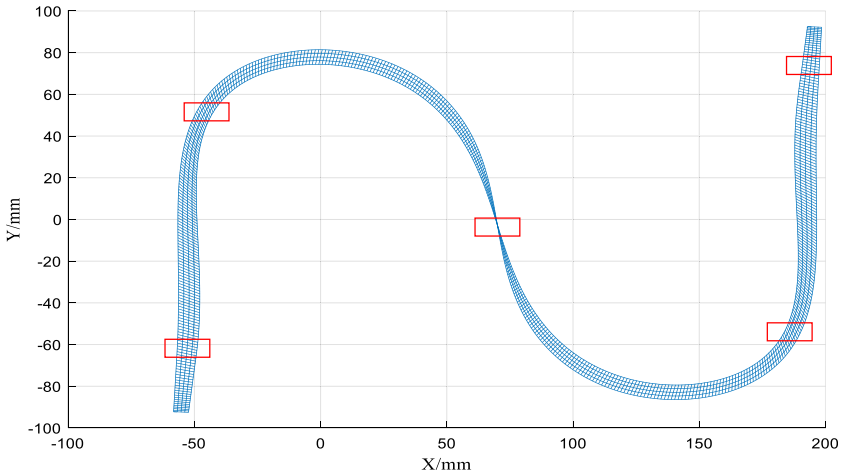

Fig. 9 The regions with a large twist on the S-shaped ruled surface

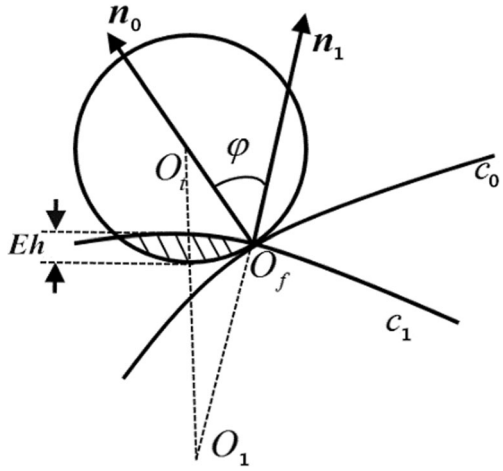

Fig. 10 Flank milling principle based on the SPO method

2.1 Directrix modeling of S-shaped test piece

At present, the B-spline surface method, Bezier surface method, Ball surface method, and Coons surface method are frequently used in CAD/CAM software. Because of geometric invariance, continuity, and symmetry, the B-spline surface method is widely applied in the field of machine design. Therefore, the uniform double cubic B-spline curve is applied to the characterization of directrix for S-shaped test piece, which is expressed as follows:

$$Q(u) = \sum_{i=0}^{n} d_i N_{i,k}(u) \tag{1}$$

where k represents the degree of B-spline curve, u represents the variable of B-spline curve ($0 \le u \le 1$), d_i represents the control points which affect the shape of the curve ($i = 0, 1, 2, ..., n$), and $N_{i,k}(u)$ represents the basis functions with k power of u, which are the core of B-spline curve.

In addition, the Cox-de Boor method proposed in [37] is employed to establish the basis functions of the B-spline curve, so the Cox-de Boor recursion formulas of basis functions are obtained as follows:

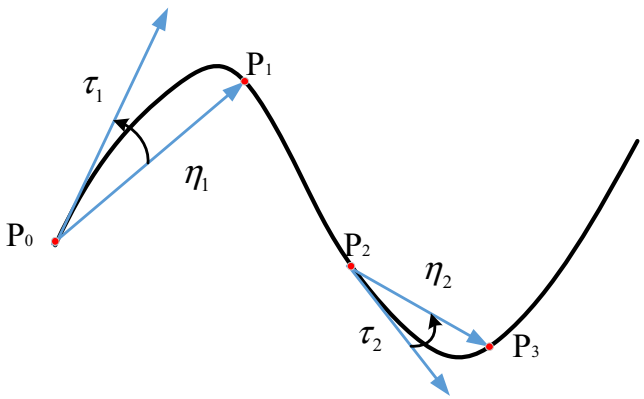

Fig. 11 The schematic diagram of the concavity and convexity

$$\begin{cases} N_{i,0} = \begin{cases} 1 & u \in [u_i, u_{i+1}] \\ 0 & \text{others} \end{cases} \\ N_{i,k}(u) = \dfrac{u-u_i}{u_{i+k}-u_i} N_{i,k-1}(u) + \dfrac{u_{i+k+1}-u}{u_{i+k+1}-u_{i+1}} N_{i+1,k-1}(u) \quad k > 0 \\ \text{In particular}: \dfrac{0}{0} = 0 \end{cases} \tag{2}$$

Since the B-spline curve data points are subject to equidistant distribution, the basis functions are expressed as follows:

$$\begin{cases} N_{0,3}(u) = \dfrac{1}{6}(1-u)^3 \\ N_{1,3}(u) = \dfrac{1}{6}\left(3u^3 - 6u^2 + 4\right) \\ N_{2,3}(u) = \dfrac{1}{6}\left(-3u^3 + 3u^2 + 3u + 1\right) \\ N_{3,3}(u) = \dfrac{1}{6}u^3 \end{cases} \tag{3}$$

On the basis of above-mentioned equations, the uniform double cubic B-spline curve with the form of the matrix is obtained, as illustrated below:

$$Q_i(u) = \frac{1}{6}\begin{bmatrix} u^3 & u^2 & u & 1 \end{bmatrix} \begin{bmatrix} -1 & 3 & -3 & 1 \\ 3 & -6 & 3 & 0 \\ -3 & 0 & 3 & 0 \\ 1 & 4 & 1 & 0 \end{bmatrix} \begin{bmatrix} d_i \\ d_{i+1} \\ d_{i+2} \\ d_{i+3} \end{bmatrix} \quad (i = 1, 2, \ldots, n-1) \tag{4}$$

Accordingly, the first point of each segment curve can be obtained as follows:

$$Q_i = Q_i(0) = \frac{1}{6}(d_i + 4d_{i+1} + d_{i+2}) \quad i = 1, 2, \ldots, n-1 \tag{5}$$

The last point of the last curve can be obtained as follows:

$$Q_n = d_{n+2} \tag{6}$$

The basis functions on the first two segments and the last two segments are different. The other segments have the same one. They are shown in references [21, 26]. So the following formula can be obtained:

$$\begin{cases} Q_1 = d_1 \\ Q_2 = \dfrac{1}{4}d_2 + \dfrac{7}{12}d_3 + \dfrac{1}{6}d_4 \\ Q_i = \dfrac{1}{6}d_i + \dfrac{2}{3}d_{i+1} + \dfrac{1}{6}d_{i+2} \quad (i = 3, 4, \ldots, n-2) \\ Q_{n-1} = \dfrac{1}{6}d_{n-1} + \dfrac{7}{12}d_n + \dfrac{1}{4}d_{n+1} \\ Q_n = d_{n+2} \end{cases} \tag{7}$$

Therefore, based on the above equations, control points of the S-shaped directrix are calculated, as shown in Fig. 2. Then, the S-shaped directrix can be obtained by means of substituting control points into Eq. (4). As illustrated in Fig. 3.

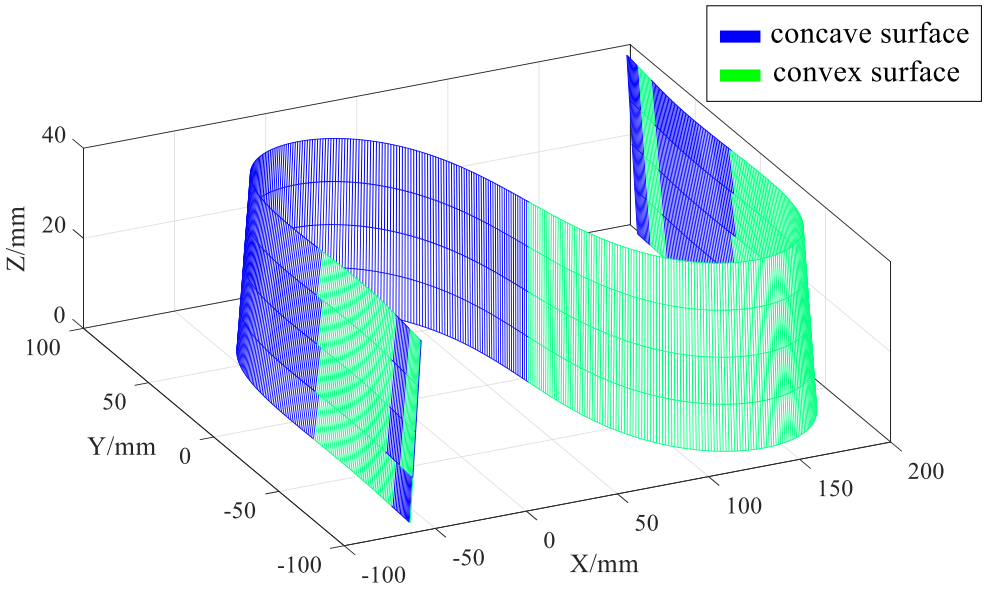

Fig. 12 Concavity and convexity of S-shaped test piece

2.2 S-shaped surface modeling

S-shaped surface belongs to a kind of non-developed rule surface, which was formed by generatrix moves along the upper and lower directrix as illustrated in Fig.4.

So the S-shaped ruled surface is expressed as follows:

$$\mathbf{L}(e,f) = (1-f)\mathbf{a}_i(e) + f\mathbf{b}_i(e) \tag{8}$$

where e represents the direction variable along directrix, f represents the direction variable along generatrix, $\mathbf{a}_i(e)$ represents the lower directrix vector, and $\mathbf{b}_i(e)$ represents the upper directrix vector.

Meanwhile, the generatrix of the ruled surface and the mesh of ruled surface are displayed in Figs. 5 and 6, respectively.

Then, the S-shaped test piece model can be established by means of the isometric thickening modeling method, which is illustrated in Fig. 7.

3 Theoretical error analysis of S-shaped test piece

The theoretical error is caused by the existence of a twist angle and the fact that the radius of the tool is not equal to zero. As shown in Figs. 10 and 14, due to the existence of twist angle, i.e., φ, φ_1, and φ_2, the direction vector of non-developed rule surface along the generatrix varies unevenly during the process of modeling of S-shaped test piece, i.e., $n_0 \neq n_1 \neq n_2$. And it can only ensure that the normal vector of non-developed rule surface coincides with the normal vector of tool surface at one point in the actual flank milling process of S-shaped test piece. Thus, it is obvious that the theoretical error cannot be averted due to the presence of twist angle in the actual flank milling processes of S-shaped test piece. Therefore, it is a prerequisite to analyze the influence of twist angle on theoretical error for improving the machining accuracy of the S-shaped test piece.

The twist angle is generated by the projection of the unit normal vector of any two directrices in the XY plane.

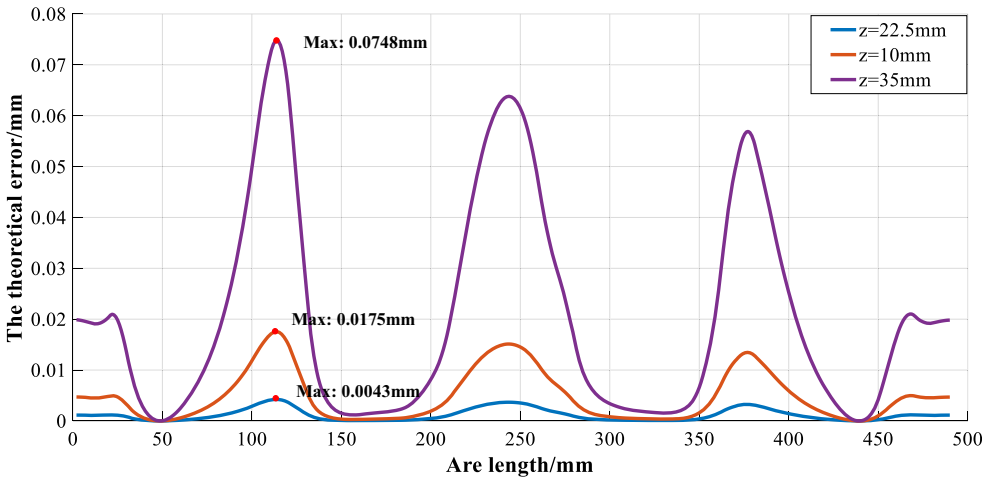

Fig. 13 The theoretical errors obtained using the SPO method

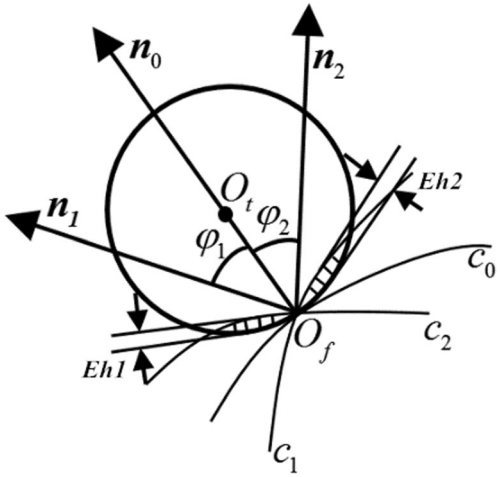

Fig. 14 Flank milling principle based on the OSPO method

Supposing that any two directrices of non-developed rule surface are expressed by $Q_1(e) = (x_1(e), y_1(e))$ and $Q_2(e) = (x_2(e), y_2(e))$, respectively. So the unit normal vectors of $Q_1(e)$ and $Q_2(e)$ are obtained, respectively, as illustrated below:

$$\mathbf{n}_1 = \left(\frac{y_1'(e)}{\sqrt{\left((x_1'(e))^2 + (y_1'(e))^2\right)}}, -\frac{x_1'(e)}{\sqrt{\left((x_1'(e))^2 + (y_1'(e))^2\right)}} \right) \tag{9}$$

$$\mathbf{n}_2 = \left(\frac{y_2'(e)}{\sqrt{\left((x_2'(e))^2 + (y_2'(e))^2\right)}}, -\frac{x_2'(e)}{\sqrt{\left((x_2'(e))^2 + (y_2'(e))^2\right)}} \right) \tag{10}$$

The twist angle can be obtained by considering Eqs. (9) and (10), as illustrated below:

Table 2 The comparison of twist angle and theoretical error

	The twist angle (°)		The theoretical error (mm)	
	SPO	OSPO	SPO	OSPO
L1	1.5912	0.4133	0.0043	0.00028
L2	3.2305	1.952	0.0175	0.00634
L3	6.6509	3.4322	0.0748	0.0191

$$\varphi = \arccos\left(\frac{x_1'(e)x_2'(e) + y_1'(e)y_2'(e)}{\sqrt{(x_1'(e))^2 + (y_1'(e))^2} + \sqrt{(x_2'(e))^2 + (y_2'(e))^2}} \right) \tag{11}$$

On the basis of Eq. (11), the twist angles are obtained, as illustrated in Fig. 8. It can be seen that the twist angle rises up and down with several peaks on the whole non-developed rule surface. The maximum twist angle is approximately 6.65° at $Z = 35$ mm. Fig. 9 represents the regions with larger twist angle on S-shaped ruled surface.

Flank milling principle based on the SPO method for calculating the theoretical error of the convex surface is represented in Fig. 10, where c_0 denotes the directrix which is located at tool offset point, c_1 denotes the lower directrix, n_0, n_1 denotes the unit normal vector of c_0 and c_1 at the cross point of two projection directrices respectively, O_f denotes tool offset point, O_t denotes tool axle center, and φ denotes the twist angle, the shadow area denotes the theoretical error.

Thus, the theoretical error of convex surface at the tool offset point i can be expressed as follows:

$$E_{hi} = r_t + r_{si} - \sqrt{r_{si}^2 + r_t^2 + 2r_{si}r_t\cos\varphi_i} \tag{12}$$

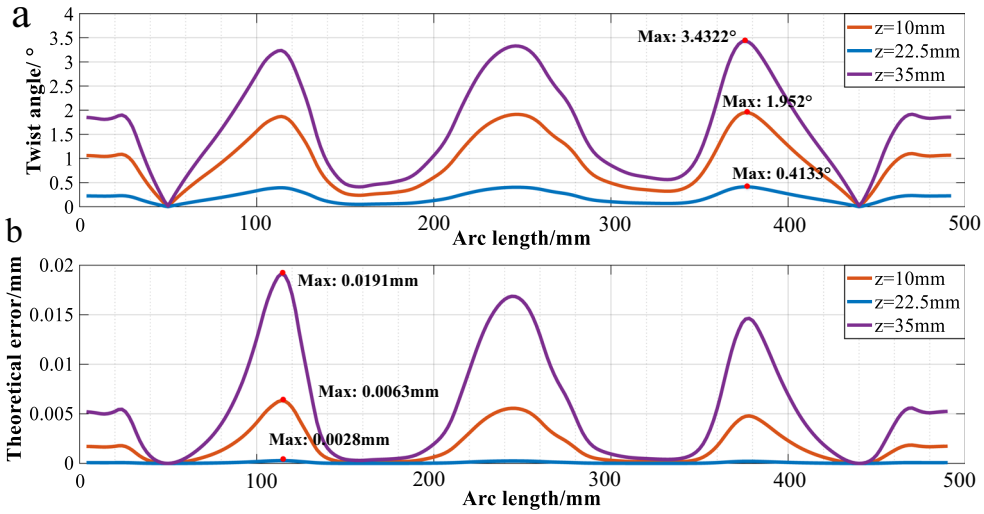

Fig. 15 **a** The twist angle of S-shaped ruled surface obtained using the OSPO method. **b** The theoretical errors obtained using the OSPO method

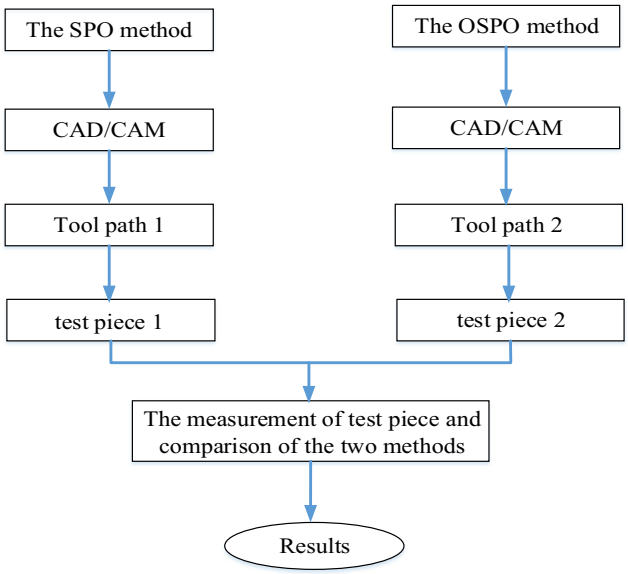

Fig. 16 The flow chart of the verification experiment

Similarly, the theoretical error of concave surface at the tool offset point i can be expressed as follows:

$$E_{li} = r_t - {}^{l}r_{si} + \sqrt{{}^{l}r_{si}{}^{2} + r_t{}^{2} - 2\,{}^{l}r_{si} r_t \cos\varphi_i} \tag{13}$$

where r_t denotes tool radius, r_{si} denotes curvature radius of the convex surface at tool offset point i, ${}^{l}r_{si}$ denotes curvature radius of the concave surface at tool offset point i, and φ_i denotes the twist angle at tool offset point i.

Then, the concavity and convexity of the surface can be calculated, as illustrated in Fig. 11 and Eq. 14.

$$\begin{cases} \boldsymbol{\eta} \times \boldsymbol{\tau} > 0 \Rightarrow \text{convex surface point} \\ \boldsymbol{\eta} \times \boldsymbol{\tau} < 0 \Rightarrow \text{concave surface point} \\ \boldsymbol{\eta} \times \boldsymbol{\tau} = 0 \Rightarrow \text{plane point} \end{cases} \tag{14}$$

Fig. 17 S-shaped test piece being machined

Fig. 18 Two test pieces produced using the SPO

where τ is the tangent vector and η is the direction vector between two points. Based on the right-hand rule of directional vector cross multiplication, if the tangent vector τ is at the position of counter-clockwise direction of direction vector η, the tool offset point is the convex surface point; otherwise, it is the concave surface point.

Thus, the concavity and convexity of the S-shaped test piece at tool offset point are obtained, as illustrated in Fig. 12.

Suppose that the tool radius is 10 mm, the single-point offset method is utilized to obtain the tool path. Then, according to Eqs. (12) and (13), the theoretical errors at different heights of S-shaped test piece are calculated, as illustrated in Fig. 13. It can be seen that the maximum theoretical errors are approximately 0.075 mm at $z = 35$ mm, which have exceeded the allowable value, i.e., $E = 0.075mm > 0.05mm$. So it is obvious that the theoretical error has significant effects when the S-shaped test piece is considered to be nearly unqualified or qualified for use. Therefore, how to develop an optimized

Fig. 19 The detecting scene of coordinate measuring machine and the OSPO methods

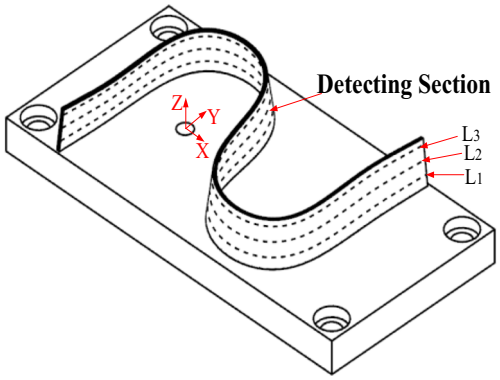

Fig. 20 Position of error detection points

single-point offset method to reduce theoretical errors is of paramount importance.

4 The optimized single-point offset (OSPO) method

In view of above-mentioned analysis, resolution strategies require a decrease in the theoretical error, and therefore, this paper proposes a method to solve this problem. In this work, the core idea of the optimized single-point offset (OSPO) method is that tool offset at one point of generatrix makes two twist angles be equal, i.e., $\varphi_1 = \varphi_2$, as illustrated in Fig. 14, where c_0 denotes the directrix which is located at tool offset point, c_1 denotes the lower directrix, and c_2 denotes the upper directrix.

Thus, the theoretical error of convex surface at the tool offset point i is expressed as follows:

$$E_{h1i} = r_t + r_{s1i} - \sqrt{r_{s1i}^2 + r_t^2 + 2r_{s1i}r_t\cos\varphi_{1i}} \tag{15}$$

$$E_{h2i} = r_t + r_{s2i} - \sqrt{r_{s2i}^2 + r_t^2 + 2r_{s2i}r_t\cos\varphi_{2i}} \tag{16}$$

$$E_{hi} = \max(E_{h1i}, E_{h2i}) \tag{17}$$

Similarly, the theoretical error of concave surface at the tool offset point i is also expressed as follows:

$$E_{l1i} = r_t - {}^{l}r_{s1i} + \sqrt{{}^{l}r_{s1i}^2 + r_t^2 - 2{}^{l}r_{s1i}r_t\cos\varphi_{1i}} \tag{18}$$

$$E_{l2i} = r_t - {}^{l}r_{s2i} + \sqrt{{}^{l}r_{s2i}^2 + r_t^2 - 2{}^{l}r_{s2i}r_t\cos\varphi_{2i}} \tag{19}$$

$$E_{li} = \max(E_{l1i}, E_{l2i}) \tag{20}$$

Therefore, the twist angle and theoretical error can be calculated based on the optimized single-point offset (OSPO) method, as illustrated in Fig. 15 a and b, respectively. According to reference [35], if the theoretical error is approximately less than 5 μm, it can be negligible. As presented in Fig. 15b, the vast majority of theoretical errors based on the OSPO method are less than 5 μm. By comparing Fig. 15b with Fig. 13, theoretical error obtained by using the OSPO method is smaller than that by using the SPO method.

As presented in Table 2, by comparing with the SPO method, the OSPO method has clear advantages in reducing twist angle and theoretical error.

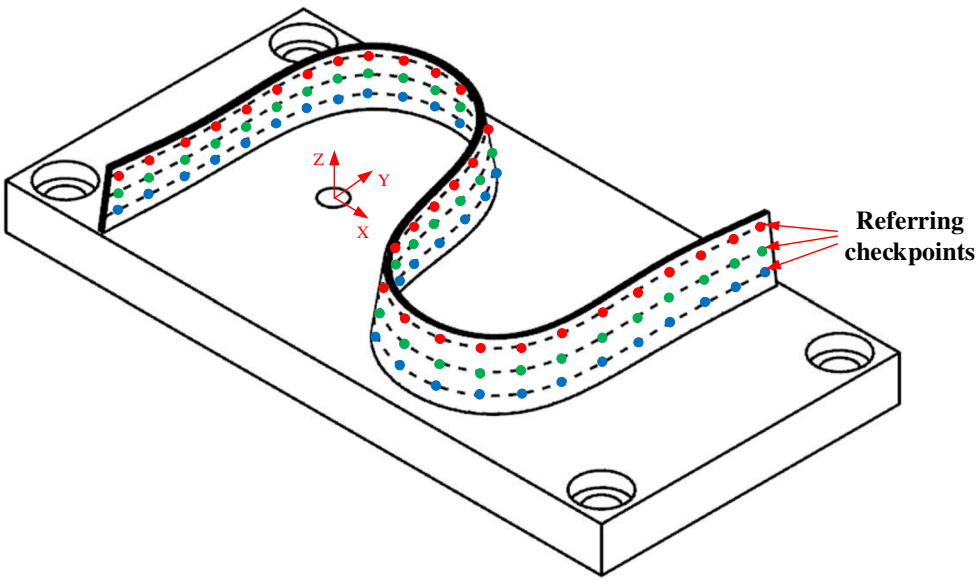

Fig. 21 Referring checkpoints schematic

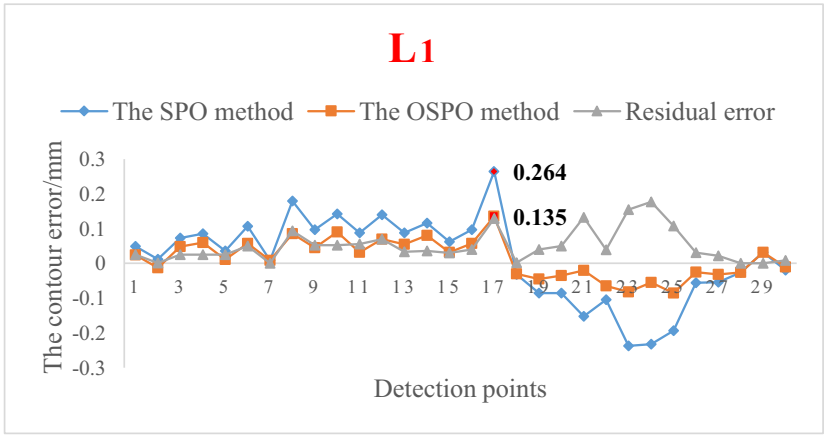

(a) The contour error of two S-shaped test pieces at L1

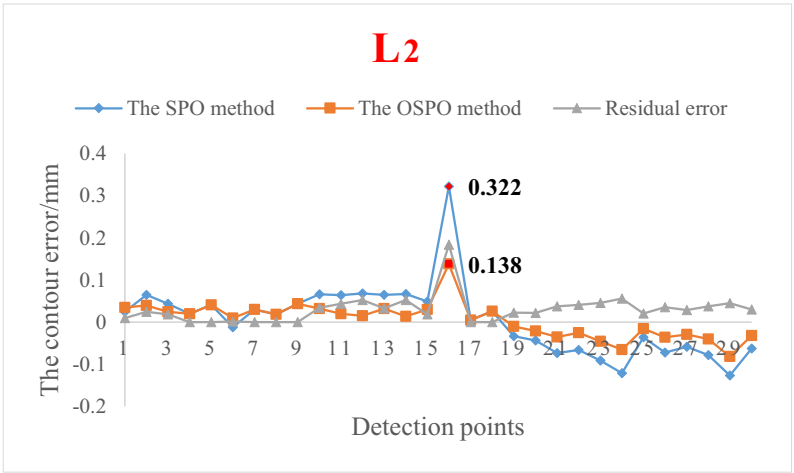

(b) The contour error of two S-shaped test pieces at L2

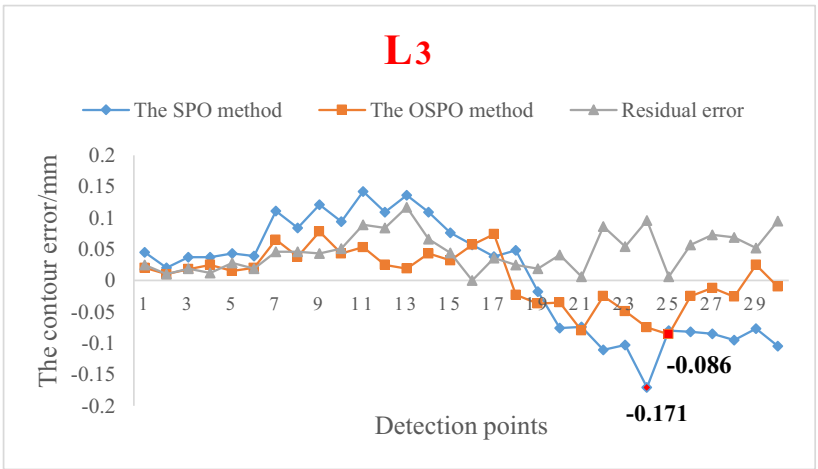

(c) The contour error of two S-shaped test pieces at L3

Fig. 22 The contour errors of two S-shaped test pieces obtained using the SPO and OSPO methods

5 Experimental validation

In order to verify the feasibility and effectiveness of the proposed method, an experiment is carried out on the gantry-type five-axis milling machine tools (XKAS2525) and coordinate measuring machine (CMM). The experiment mainly includes two parts: machining and measurement of S-shaped test piece. Fig. 16 shows the flow chart of the verification experiment.

Table 3 The comparison of average contour errors for S-shaped test piece

	Average contour error (mm) The SPO method	The OSPO method	Reduction (%)
L1	0.098	0.048	51.1
L2	0.063	0.034	46.04
L3	0.081	0.038	53.1

The dimensions and material parameters of the S-shaped test piece are displayed in Table. 1. The ϕ20-mm cylindrical milling cutter is utilized to process the S-shaped test piece. Before the machining test, tool path should be obtained. Tool path planning in this paper is carried out by CAD/CAM software based on the OSPO method. The cutter location file is subsequently generated by the post process module of Pro/E software. Before the cutting test, the NC codes with the iterative compensation methodology presented in reference [3] based on the same compensation strategy are obtained. Then, the flank milling experiment is carried out. The machining site is as illustrated in Fig. 17. Two S-shaped test pieces being machined under the same processing conditions based on the SPO method and the OSPO method are obtained respectively, as shown in Fig. 18. Finally, the contour errors of two test pieces are measured by the coordinate measuring machine (CMM) named PRISMO 125751, which is produced by the German company Zeiss. A ϕ1-mm ruby sphere with stylus length of 40 mm is used in this measurement experiment. Fig. 19 represents the scenes of measurement with a coordinate measuring machine. Three test lines are taken along the Z direction of the S-shaped edge strip, as illustrated in Fig. 20. The distance from L3 to the edge strip top is 5 mm in the Z direction. The interval of the test lines is 12.5 mm. So the recommended measurement points, which located on the L1, L2, and L3, are selected for evaluating the machining performance of five-axis machine tools. The accuracy of the whole surface can be comprehensively examined by the selected three lines. For measuring machining errors, each height is chosen at 30 equidistant discrete points. The referring checkpoint schematic in the CMM system is displayed in Fig. 21.

Before machining, NC machine tools need to warm-up for half an hour. In the measuring process, to reduce the effect of environment temperature on the measurement results, the ambient temperature is kept in the range of 20–22 °C. Moreover, in order to improve the measurement stability, the measurement of kinematic errors was carried out three times, and then the ultimate error values are the average results of three times measured values.

Therefore, the contour errors of 90 points for two S-shaped test pieces at L1, L2, and L3 based on the SPO method and the OSPO method are all obtained, as shown in Fig. 22a–c, respectively. It can be seen that the contour errors of all 90 points obtained by using the OSPO method are much smaller than that obtained by using the SPO method. The negative value denotes overcut error; conversely, the positive value denotes undercut error. The maximum contour error is decreased from 0.264 to 0.135 mm, from 0.322 to 0.138 mm, and from 0.171 to 0.086 mm at L1, L2, and L3 respectively, as illustrated in Fig. 22a–c. In addition, in order to reflect the superiority of the OSPO method more intuitively, the comparison of average contour error for S-shaped test pieces based on the SPO method and the OSPO method is shown in Table 3. It can be clearly seen that the average contour error is reduced from 0.098 to 0.048 mm, from 0.063 to 0.032 mm, and from 0.081 to 0.038 mm at L1, L2, and L3 respectively. In other words, the contour error of S-shaped test pieces based on the OSPO method is reduced by about 51.1%, 46.04%, and 53.1% at L1, L2, and L3 respectively. The average reduction based on the OSPO method is about 50.1%. According to the requirement of United States Patent, the allowable value of machining error of the S-shaped test piece is restricted within $\pm$0.05 mm, as shown in reference [19]. On the basis of the measurement results, only the test piece 2 can meet the accuracy requirements. Therefore, it is obvious that the proposed OSPO method is precise and effective to reduce the theoretical error of S-shaped test piece. The performance for various kinds of multi-axis machine tools can be accurately exhibited by S-shaped test piece based on the OSPO method.

6 Conclusion

In this paper, the optimized single-point offset (OSPO) method is proposed to reduce the theoretical error of S-shaped test piece, which has an influence on the precision acceptance of multi-axis machine tools. For the sake of the effective implementation of the method, firstly, the uniform double cubic B-spline surface model is applied to the characterization of the curved surface. By using this model, a three-dimensional model of the S-shaped test piece is established. Then, the theoretical error of S-shaped test piece caused by a twist angle is analyzed. Moreover, to reduce the theoretical error of S-shaped test piece, an optimized tool path offset method, the optimized single-point offset (OSPO) method, was proposed based on traditional single-point offset (SPO) method. In contrast to the SPO method quantitatively, the OSPO method has clear advantages in decreasing theoretical error. Finally, in order to verify the effectiveness and feasibility of the proposed method, a machining and measurement experiment is carried out. Experimental results show the theoretical error of S-shaped test piece based on the OSPO method is reduced by about 51.1%, 46.04%, and 53.1% at L1, L2, and L3 respectively, compared with that based on the SPO method. Furthermore, the average theoretical error of S-shaped test

pieces based on the OSPO method is reduced by about 50.1%. Furthermore, most of the theoretical errors based on the OSPO method are approximately less than 5 μm, which can be negligible. Therefore, there is no doubt that this method is feasible and effective enough for reducing the theoretical error. Thus, the performance of multi-axis machine tools can be comprehensively and accurately exhibited by S-shaped test piece based on the proposed method in this paper. The basic idea of the proposed method can be applied to various sculpture surfaces to effectively reduce theoretical errors.

Funding information This work is financially supported by the National Natural Science Foundation of China (No. 51775010 and 51705011) and Science and Technology Major Projects of High-end CNC Machine Tools and Basic Manufacturing Equipment of China (No. 2016ZX04003001).

References

1. Wu CJ, Fan JW, Wang QH, Pan R, Tang YH, Li ZS (2018) Prediction and compensation of geometric error for translational axes in multi-axis machine tools. Int J Adv Manuf Technol 95: 3413–3435
2. Pezeshki M, Arezoo B (2016) Kinematic errors identification of three-axis machine tools based on machined work pieces. Precis Eng 43:493–504
3. Wu C, Fan J, Wang Q, Chen D (2018) Machining accuracy improvement of non-orthogonal five-axis machine tools by a new iterative compensation methodology based on the relative motion constraint equation. Int J Mach Tools Manuf 124(1):80–98
4. Chen D, Dong L, Bian Y, Fan J (2015) Prediction and identification of rotary axes error of non-orthogonal five-axis machine tool. Int J Mach Tool Manu 94:74–87
5. Gao HM, Fang FZ, Zhang XD (2014) Reverse analysis on the geometric errors of ultra-precision machine. Int J Adv Manuf Technol 73:1615–1624
6. Fan J, Tao H, Wu C, Pan R, Tang Y, Li Z (2018) Kinematic errors prediction for multi-axis machine tools' guideways based on tolerance. Int J Adv Manuf Technol 98(5–8):1131–1144
7. Qiao Y, Chen YP, Yang JX, Chen B (2017) A five-axis geometric errors calibration model based on the common perpendicular line (CPL) transformation using the product of exponentials (POE) formula. Int J Mach Tools Manuf 118-119:49–60
8. Cheng Q, Qi BB, Liu ZF, Zhang CX, Xue DY (2019) An accuracy degradation analysis of ball screw mechanism considering time-varying motion and loading working conditions. Mech Mach Theory 134:1–23
9. He GY, Sun GM, Zhang HS, Huang C, Zhang DW (2017) Hierarchical error model to estimate motion error of linear motion bearing table. Int J Adv Manuf Technol 93:1915–1927
10. Chen G, Liang Y, Sun Y, Chen W, Wang B (2013) Volumetric error modeling and sensitivity analysis for designing a five-axis ultra-precision machine tool. Int J Adv Manuf Technol 68(9–12):2525–2534
11. Chen GS, Mei XS, Li HL (2013) Geometric error modeling and compensation for large-scale grinding machine tools with multi-axes. Int J Adv Manuf Technol 69(9–12):2583–2592
12. Feng W, Yao X, Azamat A, Yang J (2015) Straightness error compensation for large CNC gantry type milling centers based on B-spline curves modeling. Int J Mach Tools Manuf 88:165–174
13. Hong C, Ibaraki S, Matsubara A (2011) Influence of position-dependent geometric errors of rotary axes on a machining test of cone frustum by five-axis machine tools. Procedia Eng 35:1–11
14. Bi Q, Huang H, Sun C, Wang Y, Zhu L, Ding H (2015) Identification and compensation of geometric errors of rotary axes on five-axis machine by on-machine measurement. Int J Mach Tools Manuf 89:182–191
15. Zha J, Xue F, Chen YL (2017) Straightness error modeling and compensation for gantry type open hydrostatic guideways in grinding machine. Int J Mach Tools Manuf 112:1–6
16. ISO 10791-7 (2014) Test conditions for machining centres—part 7: accuracy of a finished test piece, pp 1–14
17. NAS 979 (1969) Uniform cutting test, NAS series, metal cutting equipment specifications, pp 34–7
18. Lamikiz A, Lopez L, Celaya A (2009) Machine tools for high performance machining[M]. Springer London Ltd, London, pp 219–260
19. Song ZY, Cui YW (2011) S-shape detection test piece and a detection method for detection the precision of the numerical control milling machine. United States, Invention Patent, US8061052B2
20. Zhong L, Bi Q, Huang N, Wang Y (2018) Dynamic accuracy evaluation for five-axis machine tools using S trajectory deviation based on R-test measurement. Int J Mach Tools Manuf 125:20–33
21. Wang W, Jiang Z, Li Q, Tao W (2015) A new test part to identify performance of five-axis machine tool-part I: geometrical and kinematic characteristics of S part. Int J Adv Manuf Technol 79(5):729–738
22. Wang W, Jiang Z, Li Q, Tao W (2015) A new test part to identify performance of five-axis machine tool-part II: validation of s part. Int J Adv Manuf Technol 79(5):739–756
23. Chen D, Wang H, Pan R, Fan J, Cheng Q (2017) An accurate characterization method to tracing the geometric defect of the machined surface for complex five-axis machine tools. Int J Adv Manuf Technol 93:3395–3408
24. Su Z, Wang L (2015) Latest development of a new standard for the testing of five-axis machine tools using an s-shaped test piece. Proc IMechE B J Eng Manuf 229(7):1221–1228
25. Ibaraki S, Sawada M, Matsubara A, Matsushita T (2010) Machining tests to identify kinematic errors on five-axis machine tools. Procedia Eng. 34:387–398
26. Jiang Z, Ding J, Song Z, Du L, Wang W (2016) Modeling and simulation of surface morphology abnormality of 'S' test piece machined by five-axis CNC machine tool. Int J Adv Manuf Technol 85:2745–2759
27. Marciniak K (1991) Geometric modelling for numerically controlled machining. Oxford University Press, Oxford
28. Rubio DW, Lagarrigue P, Dessein G, Pastor F (1998) Calculation of tool paths for a torus mill on free-form surfaces on five-axis machines with detection and elimination of interference. Int J Adv Manuf Technol 14(1):13–20
29. Redonnet JM, Rubio W, Dessein G (1998) Side milling of ruled surfaces: optimum positioning of the milling cutter and calculation of interference. Int J Adv Manuf Technol 14(7):459–465
30. Monies F, Felices JN, Rubio W, Redonnet JM, Lagarrigue P (2002) Five-axis NC milling of ruled surfaces: optimal geometry of a conical tool. Int J Prod Res 40(12):2901–2922
31. Bedi S, Mann S, Menzel C (2003) Flank milling with flat end milling cutters. Comput Aided Des 35(3):293–300
32. Lartigue C, Duc E, Affouard A (2003) Tool path deformation in 5-axis flank milling using envelope surface. Comput Aided Des 35: 375–382
33. Pechard PY, Tournier C, Lartigue C, Lugarini JP (2009) Geometrical deviations versus smoothness in 5-axis high-speed flank milling. Int J Mach Tools Manuf 49:454–461

34. Gong H, Cao LX, Liu J (2005) Improved positioning of cylindrical cutter for flank milling ruled surfaces. Comput Aided Des 37:1205–1213
35. Guan L, Jiao Mo J, Fu M, Wang L (2017) Theoretical error compensation when measuring an S-shaped test piece. Int J Adv Manuf Technol 93:2975–2984
36. Guan LW, Mo J, Fu M, Wang LP (2017) An improved positioning method for flank milling of s-shaped test piece. Int J Adv Manuf Technol 92(1–4):1349–1364
37. Yamaguchi F (1988) Curves and surfaces in computer aided geometric design. Springer, Berlin